iConclusions https://iconclusions.com/ Conclusions in Engineering

A Comprehensive Study of Magnetohydrodynamic Blood Flow in a Time-Invariant Porous Artery with Multi-Irregular Stenoses

Muhammad Fahim,[1, a)] **Muhammad Sajid**,[1] and **Nasir Ali**[1]

Department of Mathematics and Statistics, International Islamic University, Islamabad, Pakistan

ABSTRACT: This work investigates the impacts of mass and heat transport on blood flow in a time-invariant porous saturated artery with multi-irregular-shaped stenosis in an environment with a magnetic field. A generalized Newtonian Cross-fluid model is employed to describe the rheological behavior of blood. Nonlinear momentum, energy, and species concentration equations are normalized using dimensionless variables and then solved numerically by executing a finite difference scheme. Various parameters that arise during the normalization process are examined to determine their effects on flow characteristics including velocity, temperature, and mass diffusion. Our findings demonstrate that both the altitude of stenosis and the magnetic field parameters inhibit blood flow by reducing blood velocity, volume flow rate, wall shear stress, and heat dissipation while increasing flow resistance and concentration profile, with the effects of stenosis with the effects of the stenosis are more prominent than the magnetic field. In contrast, the permeability of the channel increases wall shear stress, velocity, volume flow rate, and temperature by turning down resistance and concentration profiles. Moreover, the Prandtl and Brinkmann numbers play an important role in controlling the temperature and mass distribution. A higher value of the Prandtl number leads to lower temperature distribution, while a greater value of the Brinkmann number causes higher temperature distribution. Unlike temperature, these quantities have opposite effects on the concentration profile. In addition, a higher Schmidt number indicates a higher concentration distribution, while a higher Soret number points out the opposite behavior.

Received: 31 May 2025
Accepted: 17 March 2026
DOI: https://doi.org/10.71107/qdgekh21

I. INTRODUCTION

Stenosis is a term used to describe the narrowing or constriction of a blood vessel. This can occur due to atherosclerosis or other conditions such as inflammation, trauma, or congenital abnormalities[1]. Stenosis can occur in any blood vessel in the body. However, it is most commonly seen in the arteries that deliver blood to the brain (cerebral arteries), the heart (coronary arteries), and the legs (peripheral arteries). Research into the mechanisms of blood circulation and transport phenomena in stenotic vessels has gained significant attention in recent years due to its clinical implications. It has stimulated the interest of biomechanical and applied mathematicians in studying arterial stenosis. They measured pressure and velocity as well as flow visualisation on experimental models of stenosis with idealized, symmetrical, or unsymmetrical geometry[2,3]. The advancement of medical imaging processes is paralleled by advances in computational fluid dynamics, which can now be applied using high-performance computers and new numerical techniques to perform numerical tests on subject-specific segments of the blood circulation after 3D reconstruction rather than focusing on the more or less short arterial, branched, or unbranched segments[4]. In addition, mathematical models are used to analyse the release of drugs from drug-eluting stents[5].

Because of its complicated structure and content, blood is a complex fluid with non-Newtonian behavior. Therefore, to correctly simulate blood movement in the cardiovascular system, blood's rheology must be classified as a non-Newtonian fluid. This arises from the fact that blood's viscosity is nonlinear, and it shows time-dependent properties such as elasticity and plasticity[6]. These characteristics shape how blood deforms in re-

[a)] Electronic mail: fahim.muh1@gmail.com

sponse to applied stress. Recent literature uses several non-Newtonian models to accurately describe blood rheology. The most widely applied model is the power law model[7], which describes a relation between deformation rate and shear stress as nonlinear. Nevertheless, this model is confined to a small range of shear rates and can not accurately describe the behavior of the streaming blood at extreme shear rates. In order to overcome this drawback, researchers tried other non-Newtonian fluid models that could better accommodate the complexity of blood flow. For example, Ali et al.[8] prefer the Sisko fluid model to study its behavior in streaming blood through a constricted channel created by pulsatile pressure gradients. In like manner, Priyadharshini and Ponalagusamy[9] took the Herschel Bulkley's fluid model, Akbar[10] the tangent hyperbolic fluid, whereas Subbarayudu et al.[11] the Williamson fluid model for deduction of blood flow characteristics in stenosed arteries. In addition, the literature has also analyzed other models of different natures such as the Cross model[12], second-grade fluid model[13], Carreau model[14], and Eyring Powell fluid[15] since they are suitable to represent blood flow in stenotic arteries. From all of the studied models, the Cross model turns out to be more suitable and interesting because of its simplicity and ability to accurately describe behavior of blood flow at high shear rates[16,17].

The effects of body acceleration and magnetic fields on the dynamics of blood circulation have resulted in different mathematical models. These parameters have been examined by different researchers applying computational fluid dynamics (CFD) simulation and analytical solutions in order to study their effect on pulsatile blood flow, arterial hemodynamics, magnetohydrodynamic (MHD) flow separation, blood flow through stenotic arteries etc. For example, Rathod and Tanveer[18] studied the pulsatile blood flow under circumstances of periodic body acceleration and magnetic fields. Midya et al.[19] considered the process of MHD flow separation and stated that a magnetic field could be used to prevent flow separation caused by complex flow patterns. Zaman et al.[20] explored the pulsatile motion of blood in a stenotic artery, incorporating the effects of both a magnetic field and a porous medium. Their findings indicated that as the strength of the magnetic field increases, the velocity of blood flow decreases while resistance rises. Awrejcewicz et al.[21] performed a study of the blood flow associated with the action of the external magnetic field, the oscillating pressure gradients, and periodic body acceleration. Mishra and Shekhawat[22] numerically simulated the internal magnetic field effect on hemodynamics in stenosed arteries. Furthermore, a numerical simulation of the bloodstream in a stenotic blood vessel subjected to an externally applied magnetic field and body acceleration was carried out by Abbas et al.[23]. Eldesoky et al.[24] treated blood as a Newtonian electrically conducting fluid and employed the generalized differential quadrature method (GDQM) to investigate magnetohydrodynamic unstable blood flow through a porous medium. In all these studies, various aspects of flow characteristics were examined and these studies have given useful insight about the complexities of blood flow under stenosis and in external fields. These results are potentially relevant in the development of novel cardiology for the detection and treatment of vascular disorders.

Studies on the transfer of heat and chemical reaction in blood flow have attracted attention of many investigators as these may be used to aid in understanding and development of arterial diseases. Caro et al.[25] proposed one hypothesis that the process of atherosclerosis could be aided by a shear dependent mass transfer between adhered blood cholesterol and the vessel wall. Moreover, Ethier[26] investigated the connection between the transport of mass and atherosclerosis through computational models. Back et al.[27] relied on computer simulations to investigate the impact of mass distribution on two-dimensional unstable blood flow via a coronary artery. Charm et al.[28] carried out experiments to investigate the diffusion of heat in small ducts. Sharma et al.[29] investigated the spatial distributions of heat and mass of the circulatory system under the influence of Joule heating and viscous dissipation. Sinha et al.[30] examined the combined impacts of MHD heat transfer and thermal radiation on blood flow through a capillary. Other investigations on mass diffusion in streaming blood stenotic arteries through axisymmetric and asymmetric models have been performed by Refs.[31–37].

In the present research, the main focus is to examine the combined impacts of both mass and heat transfer on blood streaming through a permeable artery with multiple stenoses. The rheology of blood is characterised using the Cross fluid model, which describes the viscosity of hemorheological suspensions without time dependency. This study also includes the effects of viscous dissipation on the distribution of heat and mass, which are often neglected in similar research. Furthermore, the interrelation between mass transfer and temperature changes is explained by the coupling of energy and concentration equations. The paper is organised as follows: Section 2 illustrates the flow geometry; Section 3 presents the modelling of the problem; Section 4 formulates the non-dimensional representation; Section 5 focuses on the numerical algorithm; Section 6 discusses the outcomes; and Section 7 summarises the key con-

clusions.

II. FLOW GEOMETRY

The flow geometry in this study is characterised by a non-flexible, permeable vessel with multiple stenoses. The vessel can be visualised as a solid tube with a fixed shape and dimensions. The presence of stenoses, which are constrictions or narrowings in the arterial wall, creates regions of reduced cross-sectional area within the vessel. These stenotic regions may vary in terms of their size, shape, and location along the vessel length. The irregularities in the vessel geometry caused by the stenoses give rise to variations in the flow velocity and other flow properties along the axial direction. At the vessel wall, a no-slip condition is applied, meaning that the velocity of the blood flow is zero. This condition signifies that the blood is stationary and in direct contact with the vessel wall. Furthermore, at the vessel wall, the concentration of substances in the blood, such as solutes or particles, is believed to be zero. In addition, the temperature of the vessel wall, denoted as T_w, is considered constant throughout the flow analysis. This constant wall temperature serves as a boundary condition that affects the heat transfer characteristics of the blood flow. The mathematical expression of the stenotic segment, illustrated in Figure Figure 1, is given as:

$$R(z)=\begin{cases} a-\dfrac{2\delta}{l}(z-d_1), & d_1 \le z < d_1+\dfrac{l}{2}, \\ a+\dfrac{2\delta}{l}(z-d_1-l), & d_1+\dfrac{l}{2} \le z < d_1+l, \\ a-\delta+\dfrac{4\delta}{l^2}\left(z-d_1-\dfrac{3l}{2}\right)^2, & d_1+l \le z < d_1+2l, \\ a, & \text{otherwise.} \end{cases} \tag{1}$$

III. PROBLEM FORMULATION

The narrowed vascular segment that has multiple stenoses at its lumen is developed as an L length solid tube with a circular cross-section of $2R(z)$. A polar coordinate system, designated as (r,θ,z), is utilised to depict the two-dimensional unstable bloodstream, where r embodies the radial direction, θ indicates the circumferential direction, and z advocates for the axial direction aligned with the arterial axis. The axis of symmetry of the tube is specified as $r=0$. The governing equations for this practise are the conservation of mass and Navier-Stokes equations (for describing blood motion), the energy equation (for describing heat diffusion within the blood), and the species conservation equation (for describing mass exchange within the blood), which are listed below[20]:

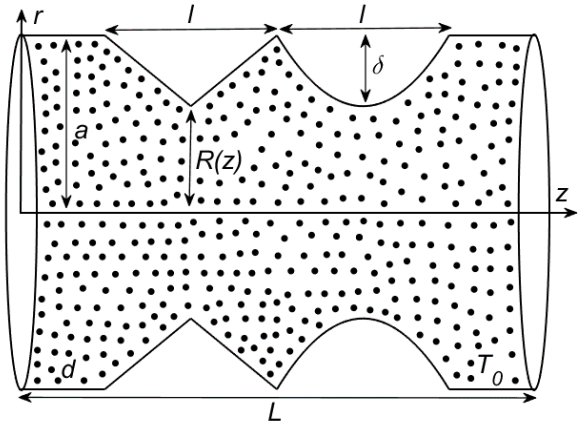

FIG. 1: Geometry of stenosed porous arterial segment.

$$\nabla\cdot\mathbf{V}=0, \tag{2}$$

$$\rho\frac{d\mathbf{V}}{dt}=-\nabla p+\nabla\cdot\mathbf{S}+\mathbf{J}\times\mathbf{B}+\frac{\mu_e\mathbf{V}}{K}, \tag{3}$$

$$\rho c_p\frac{DT}{Dt}=k_0\nabla^2T+\boldsymbol{\tau}:\nabla\mathbf{V}, \tag{4}$$

$$\frac{DC}{Dt}=D_0\nabla^2C+\frac{D_0k_t}{T_m}\nabla^2T. \tag{5}$$

In the above equations, $\boldsymbol{V}=\{u(t,r,z),0,w(t,r,z)\}$ is the velocity field, $p(r,z,t)$ is the pressure, T is the temperature, C is the concentration, $\boldsymbol{J}$ corresponds to the current density, and $\boldsymbol{B}=\boldsymbol{B}_0+\boldsymbol{B}_1$ specifies the magnetic field, in which $\boldsymbol{B}_0$ indicates a constant magnetic field applied in the radial direction, and $\boldsymbol{B}_1$ indicates the induced magnetic field. Moreover, ρ,μ_e,K, c_p,k_0,D_0,k_t, and T_m are respectively referred to blood density, the effective viscosity of porous channel, porosity coefficient, specific heat, thermal conductivity, mass diffusion coefficient, thermal diffusion coefficient, and mean temperature. By applying Ohm's law, we have:

$$\mathbf{J}\times\mathbf{B}=-\varrho\mathbf{B}_0^2\mathbf{V}. \tag{6}$$

where ϱ and $\boldsymbol{E}$ respectively, specify electric conductivity and electric field. By neglecting induced magnetic fields as well as induced and imposed electric fields[20,24], we get:

$$\boldsymbol{J}\times\boldsymbol{B}=-\varrho\boldsymbol{B}\boldsymbol{B}_0^2\boldsymbol{V}, \tag{7}$$

The Cauchy stress tensor of the Cross-fluid model can be defined as[30]:

$$\mathbf{S} = \left\{\mu_\infty + (\mu_0 - \mu_\infty)\left(1 + (\Gamma\dot{\gamma})^{n-1}\right)^{-1}\right\}\dot{\boldsymbol{\gamma}}, \quad (8)$$

where μ_0 and μ_∞ are the zero- and infinite shear rates, n is the power law index, $\boldsymbol{\gamma} = \nabla\boldsymbol{V} + (\nabla\boldsymbol{V})^t$ is the first Rivilin-Erickson tensor, and $\gamma = \sqrt{\text{trace}(\boldsymbol{\gamma})/2}$ is the second invariant of the first Rivlin-Erickson tensor. The effective viscosity, μ_e, of the porous channel for the Cross-fluid model can be defined as[31]

$$\mu_e = -\left\{\mu_\infty + (\mu_0 - \mu_\infty)\left(1 + \left(\frac{\lambda\alpha}{\sqrt{\kappa\epsilon}}|\boldsymbol{V}|\right)^{n-1}\right)^{-1}\right\}, \quad (9)$$

where α, λ, κ, and ϵ are the properties of the porous channel. The axial pressure gradient, $\partial p/\partial z$, can be defined as:

$$-\frac{\partial p}{\partial z} = A_0 + A_1\cos\omega_p t. \quad (10)$$

where A_0 and A_1 are constants that determine the magnitude of the pressure gradient. Such that A_0 represents a constant component, while A_1 represents a sinusoidal component. ω_p is the 6 angular frequency of the sinusoidal component. It is usually measured in radians per unit of time and related to the angular frequency f_p as $f_p = \omega_p/2\pi$. The supplementary conditions for the governing equations can be defined as:

The supplementary conditions for the governing equations are:

$$\begin{aligned} &w(t,r,z) = C(t,r,z) = T(t,r,z) = 0, \quad \text{at } t = 0,\\ &w(t,r,z) = C(t,r,z) = 0,\ T(t,r,z) = T_w, \quad \text{at } r = R(z),\\ &\frac{\partial w}{\partial r} = \frac{\partial C}{\partial r} = \frac{\partial T}{\partial r} = 0, \quad \text{at } r = 0. \end{aligned} \quad (11)$$

IV. NORMALIZATION OF THE PROBLEM

Normalization can make equations easier to solve and can also help to improve the stability of numerical solutions. To normalize flow equations and boundary conditions, we introduce the dimensionless variables and parameters listed below.

By using the above variables and by applying the assumption of mild stenosis and the extra condition $\epsilon \cong 1$, Eqs. (2345) are reduced to

$$\alpha\frac{\partial w}{\partial t} = -\frac{\partial p}{\partial z} + \frac{1}{r}\frac{\partial}{\partial r}(rS_{rz}) - M^2 w + \frac{\mu_e}{K}w, \quad (13)$$

$$\Pr\alpha\frac{\partial\theta}{\partial t} = Br\,S_{rz}\frac{\partial w}{\partial r} + \frac{\partial^2\theta}{\partial r^2} + \frac{1}{r}\frac{\partial\theta}{\partial r}, \quad (14)$$

$$\alpha\frac{\partial\phi}{\partial t} = \frac{1}{Sc}\left\{\frac{\partial^2\phi}{\partial r^2} + \frac{1}{r}\frac{\partial\phi}{\partial r}\right\} + Sr\left\{\frac{\partial^2\theta}{\partial r^2} + \frac{1}{r}\frac{\partial\theta}{\partial r}\right\}, \quad (15)$$

where $S_{rz} = \left\{m - (m-1)\left(1 + \left(We\left|\frac{\partial w}{\partial r}\right|\right)^{n-1}\right)^{-1}\right\}\frac{\partial w}{\partial r}$.

The dimensionless form of the stenotic section is:

$$R(z) = \begin{cases} 1 - 2\delta(z-\sigma), & \sigma \le z < \sigma + \frac{1}{2},\\ 1 + 2\delta(z-\sigma-1), & \sigma + \frac{1}{2} \le z < \sigma + 1,\\ 1 - \delta + 4\delta\left(z - \sigma - \frac{3}{2}\right)^2, & \sigma + 1 \le z < \sigma + 2,\\ 1, & \text{otherwise.} \end{cases} \quad (16)$$

where δ is the maximum altitude of stenosis and $\sigma = d_1/l$.

The dimensionless forms of the axial pressure gradient and effective viscosity of porous chennel are:

The dimensionless volumetric flow rate, wall shear stress, and resistance to flow are:

$$-\frac{\partial p}{\partial z} = \beta\{1 + e\cos(2\pi t)\}, \quad (17)$$

$$\mu_e = -\left\{m + (1-m)\left(1 + (We|w|)^{n-1}\right)^{-1}\right., \quad (18)$$

The supplementry conditions (11) are converted to

$$\begin{aligned} &w(t,r) = \phi(t,r) = \theta(t,r) = 0, \text{ at } t = 0,\\ &w(t,r) = \phi(t,r) = 0, \theta(t,r) = 1, \text{ at } r = R(z),\\ &\frac{\partial w}{\partial r} = \frac{\partial\phi}{\partial r} = \frac{\partial\theta}{\partial r} = 0, \text{ at } r = 0, \end{aligned} \quad (19)$$

One of the main objectives of studying blood flow through stenotic arteries is to understand the hemodynamic effects of narrowing and the risk of thrombosis, or atherosclerosis. Therefore, some critical flow properties to be analysed along with velocity are the volumetric flow rate (Q), wall shear stress (τ_s), and resistance to flow (Λ). The dimensionless expressions of these properties are:

$$Q = \int_0^R wr\,dr \quad (20)$$

$$\tau_s = \left[\left(m - (m-1)\left(1 + \left(We\left|\frac{\partial w}{\partial r}\right|\right)^{n-1}\right)^{-1}\right)\frac{\partial w}{\partial r}\right]_{r=R}, \quad (21)$$

$$\bar{t}=\frac{\omega_p t}{2\pi},\bar{r}=\frac{r}{a},\bar{W}=\frac{w}{U_0},\bar{Z}=\frac{z}{l},\bar{R}=\frac{R}{a},\bar{u}=\frac{lu}{\delta U_0},\bar{p}=\frac{a^2p}{\mu_0 lU_0},m=\frac{\mu_\infty}{\mu_0},\bar{S}_{\bar{r}\bar{z}}=\frac{aS_{rz}}{U_0\mu_0},\bar{S}_{\bar{r}\bar{r}}=\frac{lS_{rr}}{U_0\mu_0},\bar{S}_{\bar{z}\bar{z}}=$$
$$\frac{lS_{zz}}{U_0\mu_0},\bar{S}_{\bar{\theta}\bar{\theta}}=\frac{lS_{\theta\theta}}{\mu_0 U_0},\bar{\gamma}=\frac{a\gamma}{U_0},\bar{\delta}=\frac{\delta}{a},\theta=\frac{T}{T_w},\phi=\frac{c-c_1}{C_1},e=\frac{A_1}{A_0},\alpha=\frac{\rho a^2\omega_p}{2\pi\mu_0},\beta=\frac{A_1a^2}{\mu_0U_0},We=\frac{\Gamma U_0}{a},B_r= \tag{12}$$
$$\frac{\mu_0U_0^2}{K_0T_w},\mathrm{Pr}=\frac{\mu_0c_p}{K_0},Sc=\frac{\mu_0}{\rho D_0},Sr=\frac{\rho D_0k_TT_w}{\mu_0T_mC_1},\epsilon=\frac{a}{l}.$$

$$\Lambda=\frac{\beta(1+e\cos(2\pi t))}{\int_0^R wrdr} \tag{22}$$

In order to normalise the computational domain $(0,R(z))$, we take advantage of the following radial coordinate transformation:

$$\xi=\frac{r}{R(z)} \tag{23}$$

This transformation leaves Eqs. (13-15) to:

$$\alpha\frac{\partial\phi}{\partial t}=\left[\frac{1}{Sc}\left\{\frac{1}{R^2}\frac{\partial^2\phi}{\partial\xi^2}+\frac{1}{R}\frac{1}{\xi}\frac{\partial\phi}{\partial\xi}\right\}+Sr\left\{\frac{1}{R^2}\frac{\partial^2\theta}{\partial\xi^2}+\frac{1}{R^2}\frac{1}{\xi}\frac{\partial\theta}{\partial\xi}\right\}\right], \tag{27}$$

where supplementary conditions (19) are converted to:

$$\begin{aligned}&w(t,\xi)=\phi(t,\xi)=\theta(t,\xi)=0,\ \text{at } t=0,\\&w(t,\xi)=\phi(t,\xi)=0,\theta(t,\xi)=1,\ \text{at } \xi=1,\\&\frac{\partial w}{\partial\xi}=\frac{\partial\phi}{\partial\xi}=\frac{\partial\theta}{\partial\xi}=0,\ \text{at } \xi=0.\end{aligned} \tag{28}$$

The critical flow properties (20–22) in terms of variable (23) are:

$$Q=\frac{1}{R^2}\int_0^1 w\xi d\xi \tag{29}$$

$$\Lambda=\frac{B_1(1+e\cos(2\pi t))}{\frac{1}{R^2}\int_0^1 w\xi d\xi} \tag{31}$$

V. NUMERICAL ANALYSIS

The finite difference technique is a common method used by researchers to investigate blood flow through stenotic arteries. It is a time marching approach, meaning it solves the problem in discrete time steps. It is framed on the idea of estimating the derivatives in PDE by finite differences, and then solving the formed system of the algebraic equation. It is especially useful for time dependent variables and often very efficient for problems with small spatial domain.

In order to execute the finite difference technique, we need to discretize the space and time dimensions. Let's consider a time step Δt and a spatial step Δx, such that $t_k=(k-1)\Delta t$ and $x_j=1/(J+1)$, where k and $j(=1,2,3\ldots,J+1)$ represent discrete time and spatial indices, respectively. With the help of these discretizations, we can estimate the partial derivatives in the PDE with finite difference approximations given by:

$$\frac{\partial w}{\partial t}=\frac{w_j^{k+1}-w_j^k}{\Delta t}, \tag{32}$$

$$\frac{\partial w}{\partial\xi}=w_\xi=\frac{w_{j+1}^k-w_j^k}{2\Delta\xi}, \tag{33}$$

$$\frac{\partial^2 w}{\partial\xi^2}=w_{\xi\xi}=\frac{w_{j+1}^k-2w_j^k+w_{j-1}^k}{(\Delta\xi)^2} \tag{34}$$

By integrating these approximations into the original PDEs (24–26), we obtained the explicit finite difference equations given below:

$$\phi_j^{k+1}=\phi_j^k+\frac{\Delta t}{\alpha}\left[\frac{1}{Sc}\left\{\frac{1}{R^2}\phi_{\xi\xi}+\frac{1}{R^2}\frac{1}{\xi}\phi_\xi\right\}+Sr\left\{\frac{1}{R^2}\theta_{\xi\xi}+\frac{1}{R^2}\frac{1}{\xi}\theta_\xi\right\}\right], \tag{37}$$

where $w\,(t_{k+1},x_j)$, $\theta\,(t_{k+1},x_j)$, and $\phi\,(t_{k+1},x_j)$ are the values of the unknown functions w,θ, and ϕ at the next time step.

The supplementary conditions (27) are discretized as

$$\begin{aligned}&w_j^1=\theta_j^1=0,\ \text{at } t=0,\\&w_1^k=w_2^k,\theta_1^k=\theta_2^k,\phi_1^k=\phi_2^k,\ \text{at } x=0,\\&w_{J+1}^k=\phi_{J+1}^k=0,\theta_{J+1}^k=1,\ \text{at } x=1,\end{aligned} \tag{38}$$

A convergence criterion is necessary to decide when the numerical solution of governing equation is correct

$$\alpha\frac{\partial w}{\partial t}=\beta\{1+e\cos(2\pi t)\}+\frac{1}{R^2}\frac{1}{\xi}\frac{\partial}{\partial\xi}\left(\xi\left\{m-(m-1)\left(1+\left(We\left|\frac{1}{R}\frac{\partial w}{\partial\xi}\right|\right)^{n-1}\right)^{-1}\right\}\frac{\partial w}{\partial\xi}\right)- \\ M^2w-\frac{1}{K}\left\{m+(1-m)\left(1+(We|w|)^{n-1}\right)^{-1}\right\}w, \tag{24}$$

$$\Pr\alpha\frac{\partial\theta}{\partial t}=Br\left\{m-(m-1)\left(1+\left(We\left|\frac{1}{\xi}\frac{\partial w}{\partial\xi}\right|\right)^{n-1}\right)^{-1}\right\}\frac{\partial w}{\partial\xi}+\frac{1}{R^2}\frac{\partial^2\theta}{\partial\xi^2}+\frac{1}{R^2}\frac{1}{\xi}\frac{\partial\theta}{\partial\xi}, \tag{25}$$

enough to be useful. A criterion for the numerical solution to converge is applied in this study based on the relative error of successive iterations defined as:

$$\varepsilon=\left|w_j^{k+1}-w_j^k\right|/\left|w_j^{k+1}\right|, \tag{39}$$

where w_j^k represents the solution at the $k-th$ iteration. The numerical solution shows convergence behavior after its relative error reaches a predefined tolerance threshold (which we set at 10^{-6}. The accuracy and stability of numerical velocity solutions can be maintained through continuous evaluation of the convergence criterion. This objective metric allows both solution convergence evaluation and determination of required iteration numbers needed to achieve accuracy goals. We determined $\Delta t=0.00001$ and $\Delta x=0.025$ which provided acceptable accuracy reaching 10^{-6}.

VI. RESULTS AND DISCUSSION

To analyse the qualitative impacts of the emergent parameter on velocity, temperature, mass concentration, and other physical variables, we endorse the below set of data:

$$\alpha=1,\ \mu_0=0.56,\ \mu_\infty=0.0345,\ z=2,\ l=1,\ d_1=0.5,\\ e=0.5,\ f_p=1.2,\ a=0.5,\ n=0.7,\ \delta=0.2,\ We=0.5,\\ M=0.5,\ K=0.5,\ Pr=10,\ Br=2,\ Sr=0.5,\ Sc=0.5. \tag{40}$$

The numerical method validation was achieved by matching our results for axial velocity against published content in Refs.[24] and[31]. A direct comparison was performed on the specified parameter sets of $\{A_0=1,A_1=M=1,\delta=0,1/K=2,m=1,n=1\}$ for Ref. [24] and $\{\beta=4,\delta=0.1,n=0.7,We=0.5,M=0,1/K\to\infty\}$ for Ref. [31], and the results are plotted in Figure Figure 2. The results from our numerical system align with those presented by Refs. [24] and [31], thereby proving our system's accuracy and reliability. The agreement in profiles for axial velocity demonstrates that our approach functions reliably thus giving us greater assurance in the obtained findings.

A disrupted velocity field of blood is often characteristic of a stenosed artery, being a particular source of complications such as high blood pressure, poor oxygen supply, and thrombosis. Thus, it is important, therefore, to study the velocity field in order to understand the functionality of these arteries and to develop therapies that increase blood flow and prevent these complications. We found an intriguing tendency in the behaviour of blood velocity within the stenotic artery through numerical simulations. Our results particularly demonstrate that blood flow velocity decreases notably when magnetic fields become strong and vessel obstruction becomes more extensive, as shown in Figure 3. The blood stream encounters resistance due to rising magnetic field strength, which restricts blood movement within the artery. This occurs because the charged particles in the blood interact with the magnetic field, causing higher resistance and lower velocity. Further, blood flow characteristics are greatlyinfluenced by the extent of stenosis, or the narrowing of the artery lumen. The more severe the stenosis becomes, the smaller the area available for blood to pass through. As the stenosis becomes more severe, the available area for blood passage gets smaller. This results in a narrowing of the flow pathway and, as a result, a diminution in blood velocity. Additionally, this figure indicates that blood velocity is positively correlated with vessel wall porosity. This is because a permeable membrane allows for greater fluid exchange between the circulation and the surrounding tissue. This improves fluid movement and, consequently, increases blood velocity.

$$\alpha\frac{\partial\phi}{\partial t}=\frac{1}{Sc}\left\{\frac{1}{R^2}\frac{\partial^2\phi}{\partial\xi^2}+\frac{1}{R}\frac{1}{\xi}\frac{\partial\phi}{\partial\xi}\right\}+Sr\left\{\frac{1}{R^2}\frac{\partial^2\theta}{\partial\xi^2}+\frac{1}{R^2}\frac{1}{\xi}\frac{\partial\theta}{\partial\xi}\right\}, \tag{26}$$

$$\tau_s=\left[\frac{1}{R}\left(m-(m-1)\left(1+\left(We\left|\frac{1}{R}\frac{\partial w}{\partial\xi}\right|\right)^{n-1}\right)^{-1}\right)\frac{\partial w}{\partial\xi}\right]_{\xi=1}, \tag{30}$$

Figure 4 indicates that the Weissenberg number and the power law index both have a negative impact on blood velocity. This is because the Weissenberg number reflects the relative importance of viscoelastic effects in fluid flow, whereas the power law index illustrates the non-Newtonian behaviour of blood, capturing its shear-thinning or shear-thickening features. Consequently, both of these elements increase blood viscosity, making it more difficult for blood to circulate.

Our results demonstrate that blood flow velocity decreases notably when magnetic fields become strong and vessel obstruction becomes more extensive, as shown in Figure 3. Additionally, blood velocity is positively correlated with vessel wall porosity. Figure 4 indicates that the Weissenberg number and the power law index both have a negative impact on blood velocity. Another important component to consider when analysing blood flow through stenotic regions is the volume flow rate, which may assist in determining the severity of the stenosis, the risk of complications, and the efficacy of treatment. It is evident from Figure 5 that the volume flow rate is greatly impacted by the altitude of the stenosis. A significant reduction in volume flow rate is observed as the stenosis altitude goes up. This irregularity is analogous to the narrowing of the artery lumen caused by stenosis. In addition, this graphic also indicates that the volume flow rate decreases with increasing magnetic field strength but increases with increasing vessel wall porosity. A high-strength magnetic field can make the blood cells orient in a particular direction and, therefore, hinder their flow in the blood vessels. As a result of this, the volume flow rate drops with increasing magnetic field. On the other hand, a vessel wall that is more permeable allows for greater blood flow through the channel, increasing the volume flow rate. This is due to the ability of blood to pass through the pores of the wall, which shortens the blood's course of travel. Figure 6 depicts the connection between the volume flow rate and two critical parameters: the Weissenberg number and the power law index. The measured pattern portrays a constant decline in the volume flow rate when the Weissenberg number and the power law index are elevated. The decrease in flow rate with increasing Weissenberg numbers and power law indexes can be explained by the fact that these parameters make it more difficult for the fluid to flow. The higher their values, the harder it is for the fluid to flow, and therefore, the lower the flow rate will be. Wall shear stress (WSS) is the force imposed by blood on the arterial wall. It plays an important role in the formation and progression of atherosclerosis, a disease in which plaque accumulates in the vessel walls. In order to visualize the impacts of emergent parameters on WSS, we set up Figures 7 and 8. In Figure 7, both the Weissenberg number and the power law index show a clear trend of increasing wall shear stress. The observed progress in wall shear stress in the stenosed section due to greater Weissenberg numbers and power law indices has crucial physiological consequences. An elevated level of wall shear stress possesses the ability to produce negative effects on endothelial cells that line the arterial walls. Therefore, to assess the hemodynamic conditions in stenosed arteries and their potential role in cardiovascular disease progression, it is crucial to understand the impact of these rheological parameters on wall shear stress. Figure 8 demonstrates the variations in wall shear stress with respect to three parameters: wall porosity, stenosis size, and magnetic field. Results illustrate distinct patterns for each parameter. It is observed that the wall porosity correlates positively with wall shear stress. As porosity improves, flow resistance within the vessel reduces due to the existence of more open spaces or pores in the wall. This causes increased blood flow velocity and, as a result, increased wall shear stress. On the other hand, the stenosis size is substantially inversely related to wall shear stress. As the stenosis grows in size, the available cross-sectional area for the bloodstream diminishes significantly, resulting in a lower velocity gradient via stenotic section. This weakened velocity gradient creates a localized decrease in wall shear stress at the stenosis' narrowest location. Furthermore, there is also a negative correlation between magnetic field intensity

$$w_j^{k+1} = w_j^k + \frac{\Delta t}{\alpha}\left[\beta\{1+e\cos(2\pi t_k)\} + \frac{1}{R^2}\frac{w_\xi}{\xi}\left\{m-(m-1)\left(1+\left(We\left|\frac{1}{R}w_\xi\right|\right)^{n-1}\right)^{-1}\right\}+\right.$$
$$\frac{1}{R^2}\left\{m+(1-m)\left(1+\left(We\left|\frac{1}{R}w_\xi\right|\right)^{n-1}\right)^{-1}\right\}w_{\xi\xi} + \frac{1-m}{R^2}w_x\frac{\partial}{\partial\xi}\left(\left(1+\left(We\left|\frac{1}{R}w_\xi\right|\right)^{n-1}\right)^{-1}\right) - \tag{35}$$
$$\left. M^2 w_j^k - \frac{1}{K}\left\{m+(1-m)\left(1+\left(We\left|w_j^k\right|\right)^{n-1}\right)^{-1}\right\}w_j^k\right],$$

$$\theta_j^{k+1} = \theta_j^k + \frac{\Delta t}{\alpha}\frac{1}{Pr}\left[Br\left\{m-(m-1)\left(1+\left(We\left|\frac{1}{R}w_\xi\right|\right)^{n-1}\right)^{-1}\right\}w_\xi + \frac{1}{R^2}\theta_{\xi\xi} + \frac{1}{R^2}\frac{1}{\xi}\theta_\xi\right], \tag{36}$$

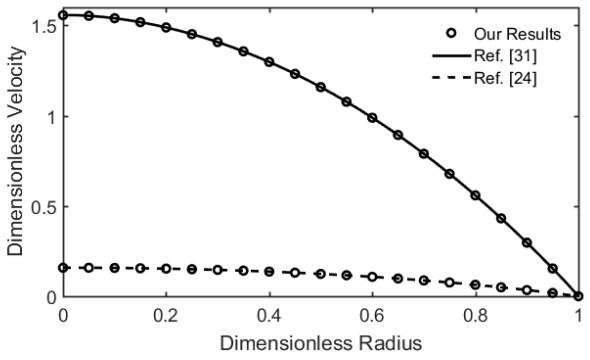

FIG. 2: Comparison of our results with previous studies[24,31].

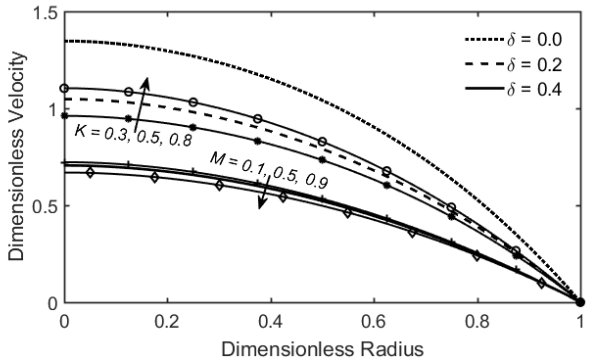

FIG. 3: Variation of velocity distribution with δ, K, and M.

and wall shear stress. When a magnetic field is imposed it acts as a restraining force on the circulating blood, causing it to slow down. This flow resistance causes a drop in velocity and, as a result, a decrease in wall shear stress. The behaviour of resistance to the flow with the variation of the altitude of stenosis, the porosity of the wall, the magnetic field, and blood rheology is demonstrated in Figures 9 and 10. The observation that resistance to flow rises with the extent of the stenosis complies with knowledge of fluid dynamics in constrained arteries. A greater degree of stenosis (narrowing) potentially results in increased resistance to flow. This is due to the vessel's restricted region acting as a bottleneck, causing blood to flow through a smaller aperture. As a result, the pressure gradient across the stenosis rises, which boosts flow resistance. The increase in flow resistance caused by stenosis can have detrimental implications. For example, it might result in reduced blood flow to tissues downstream of the stenosis, which can lead to ischemia (tissue death). Furthermore, Figure 9 shows that enhancing the potency of the magnetic field enhances flow resistance marginally. This is due to the possibility that the blood cells might be deflected by the Lorentz force, which is applied to a moving charge in a magnetic field, leading to collisions between them and the vessel walls. This can result in more frictional resistance, which might result in less blood flow. On the other hand, the opposite tendency observed with increasing porosity of the wall can be attributable to increased permeability of the vessel wall. To put it another way, better permeability allows for smoother blood flow, which reduces the amount of resistance the fluid faces when it flows. Figure 10 portrays the impacts of the power law index and the Weissinberg number on flow resistance. Since both of these elements characterise a fluid's rheology. Therefore, as the power law index, or Weissenberg number, gets higher, so does the resistance to flow. This is due to the fact that the higher

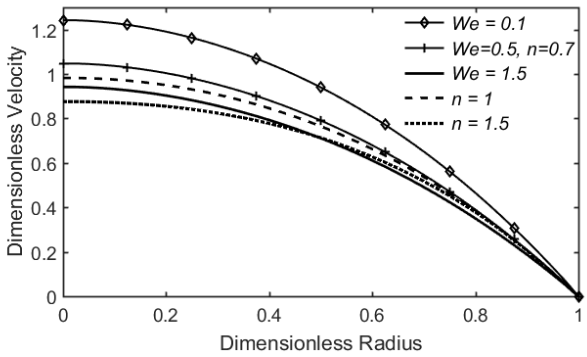

FIG. 4: Variation of velocity distribution with We and n.

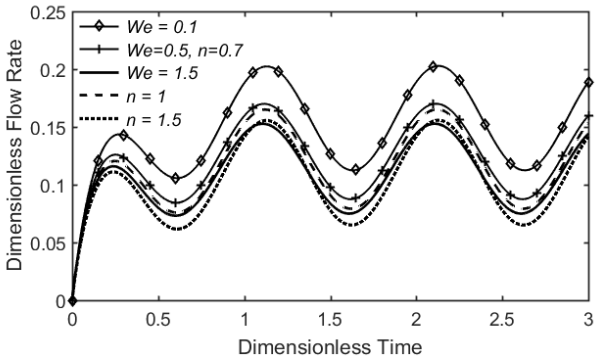

FIG. 6: Flow-rate behavior for specified values of We and n.

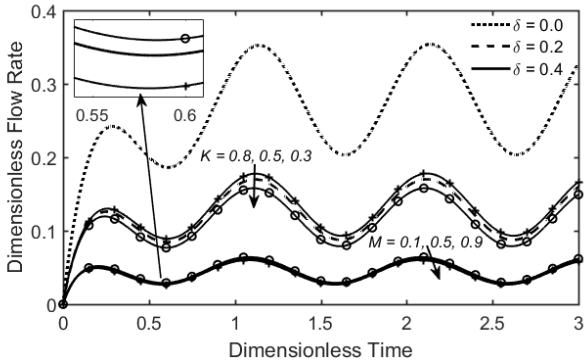

FIG. 5: Flow-rate behavior for specified values of δ, K, and M.

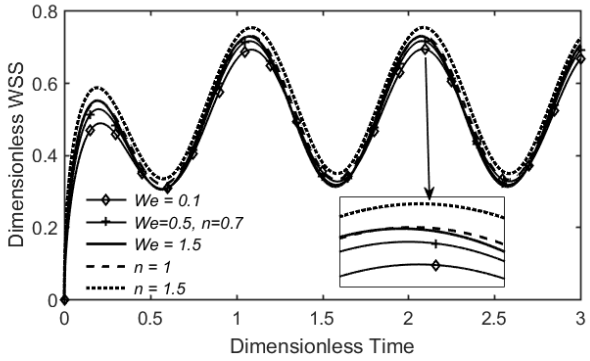

FIG. 7: WSS distribution for specific values of We and n.

the power law index, or Weissenberg number, the more elastic the fluid becomes and the more resistant it is to deformation. The temperature of the bloodstream is an essential measure that can indicate the hemodynamic and metabolic condition of the vascular system. Analyzing blood temperature via stenosed arteries can help diagnose and treat numerous cardiovascular illnesses such as atherosclerosis, thrombosis, and ischemia. Stenosed arteries are constricted or obstructed by plaque accumulation, which lowers blood flow and increases resistance and friction in the channel. This can cause local temperature fluctuations, which can be observed using a variety of approaches. To look at the impacts of various arising parameters, we projected Figures 11 to 13. The impacts of the Brinkman and Prandtl numbers are evoked in Figure 11. As the Brinkman number (Br) quantifies the ratio of heat generated via viscous dissipation to heat performed by molecular conduction, while the Prandtl number (Pr) corresponds to the ratio of momentum diffusivity to thermal diffusivity. Therefore, the temperature profile of blood increases by increasing the values of Brinkman number because more heat is generated by the friction between the blood and the vessel wall than is dissipated by conduction. This causes the blood temperature to rise closer to the wall, leading to a steep temperature gradient. The drops when the Prandtl number goes up because the thermal diffusivity of blood exceeds than its momentum diffusivity. This implies that heat can diffuse quicker than velocity, resulting in a smaller temperature difference between the wall and the bulk fluid. The variations in the blood temperature profile with respect to the altitude of stenosis, magnetic field intensity, and porosity parameter are illustrated in Figure 12. It is found that blood temperature increases significantly with an increase in stenosis altitude. The reason is that an increase in altitude leads to a reduction in the cross-sectional area available for blood flow. This forces the blood to flow through

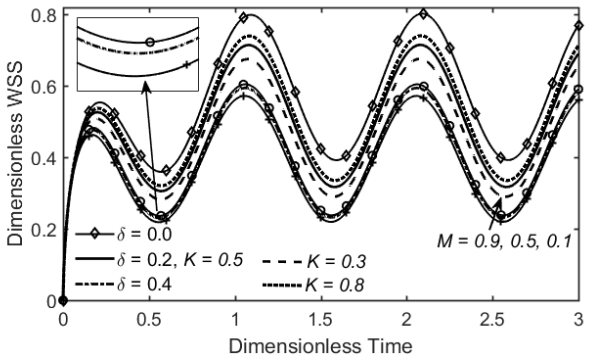

FIG. 8: WSS distribution for specific values of δ, K, and M.

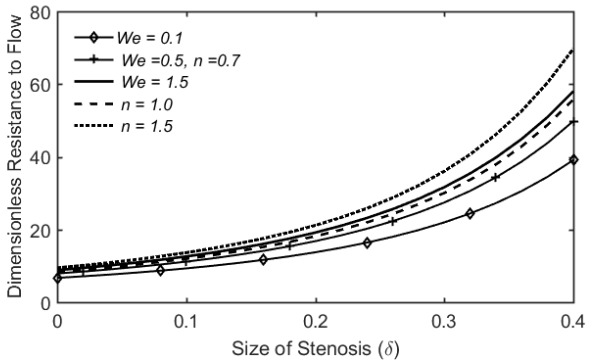

FIG. 10: Resistance to flow against δ for various We and n.

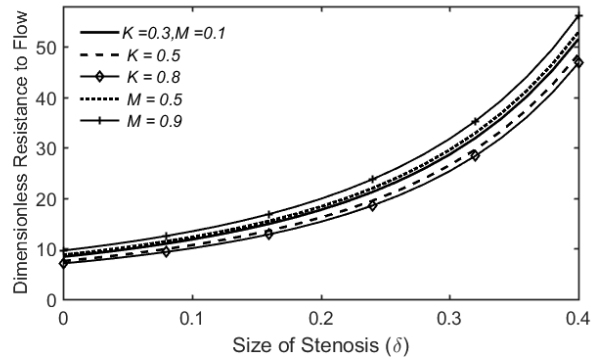

FIG. 9: Resistance to flow against δ for various M and K.

a smaller area, which increases the friction between the blood and the artery walls. The frictional forces generate heat, which can raise blood temperature. Further the temperature profile is also shown to fall somewhat when the magnetic field is increased. This is because the magnetic field causes Lorentz forces, which hinder fluid mobility and diminish thermal mixing. This results in a comparatively lower temperature profile than without a magnetic field. Finally, this graphic shows that enhancing wall porosity marginally raises the temperature profile. Increased porosity means better permeability, allowing for greater fluid exchange between the vessel lumen and its surrounding tissues. This improves the thermal connection between the blood and the vessel wall. As a result, there is a slight increase in the temperature distribution. Figure 13 depicts the temperature distribution for various Weissenberg number and power law index values. The results show that the temperature distribution enhances as We increases, implying that elastic effects improve heat transport in the fluid. However, when n increases, the temperature distribution diminishes, implying that shear-thinning processes impede heat transport in the fluid.

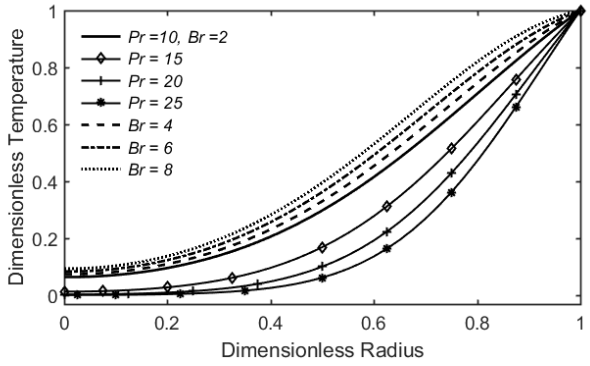

FIG. 11: Temperature profiles for particular values of Pr and Br.

Mass concentration through stenosed arteries is a complicated process influenced by various factors. These factors include the severity of the stenosis, the blood viscosity, and the vessel geometry. The concentration of mass reduces significantly when the stenosis grows in size. This can be attributed to the narrowing of the vessel lumen, which restricts flow and reduces mass transport capacity. This fact is illustrated in Figure 14. Furthermore, this graph depicts that when the porosity parameter increases, the mass concentration drops slightly due to the porous medium's improved permeability. Meanwhile, the magnetic field affects mass concentration by increasing it to some extent. Because the magnetic field induces a Lorentz force, which opposes

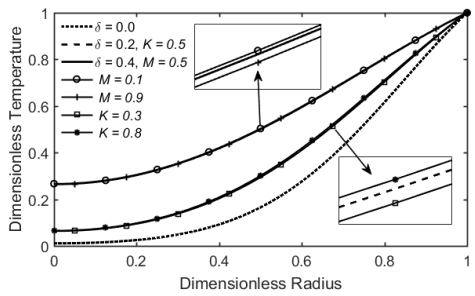

FIG. 12: Temperature profiles for particular values of δ, M, and K.

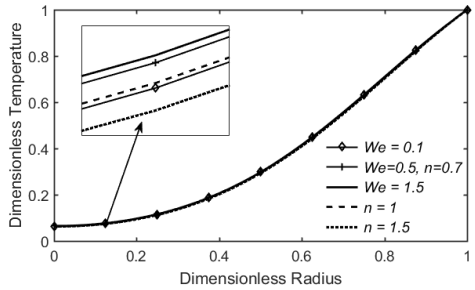

FIG. 13: Temperature profiles for particular values of We and n.

fluid velocity and prolongs particle retention time. Figure 15 examines the mass concentration in blood flow through stenotic vessels with respect to the powe law exponent and Weissenberg number. It is noted that the mass concentration exhibits a slight decrease when the Weissenberg number is increased, and a moderate increase when the power law index is increased. This indicates that fluid rheology has an effect on the mass transfer in the flow domain. Figure 16 examines the mass concentration in blood flow via stenosed arteries about the Soret and Schmidt numbers. The results illustrate that both factors have profound effects on mass concentration. The Soret number measures a solute's tendency to diffuse in the direction of a temperature gradient, whereas the Schmidt number measures the ratio of momentum diffusivity to mass diffusivity. In other words, the Soret number measures the degree to which solute concentration changes due to temperature variation. Meanwhile, the Schmidt number measures how fluid velocity impacts the concentration of a solute. As the Soret and Schmidt numbers increase, the mass concentration in blood flow spikes up because the solute is more likely to diffuse in the direction of the temperature gradient, and the fluid's velocity is more likely to drive away the solute from the source of the concentration gradient. As a result, an enhanced mass distribution occurs within the blood flow. Figure 17 illustrates the role of the Prandtl and Brinkman numbers on the characteristics of mass concentration.

Increasing the Prandtl number leads to raising the mass concentration in a stenosed region, whereas increasing the Brinkman number results in a decrease in mass concentration. In a stenosed region, fluid flow is restricted, which increases viscous force. The Prandtl number is inversely proportional to the viscous force, so enhancing the Prandtl number will decrease the viscous force and allow more mass to diffuse into the stenosed region. The Brinkman number is directly proportional to the viscous force, so increasing the Brinkman number will increase the viscous force and make it harder for mass to diffuse into the stenosed region.

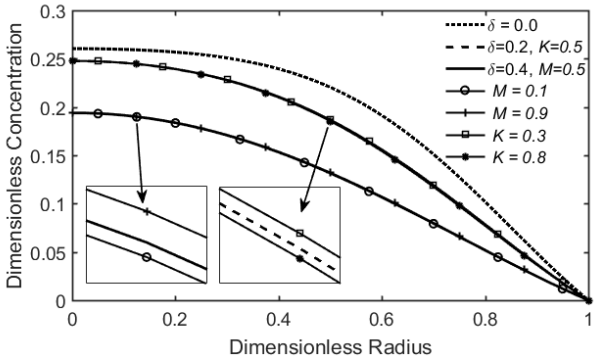

FIG. 14: Mass distribution for specific values of δ, M, and K.

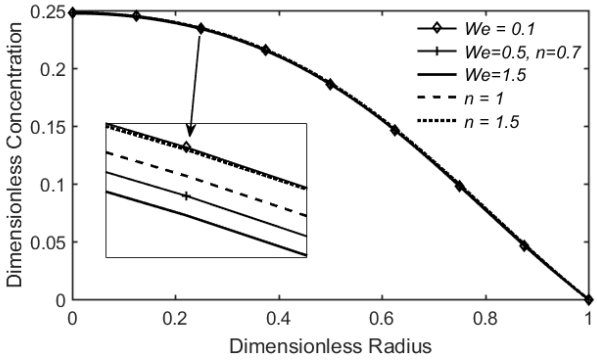

FIG. 15: Mass distribution for specific values of We and n.

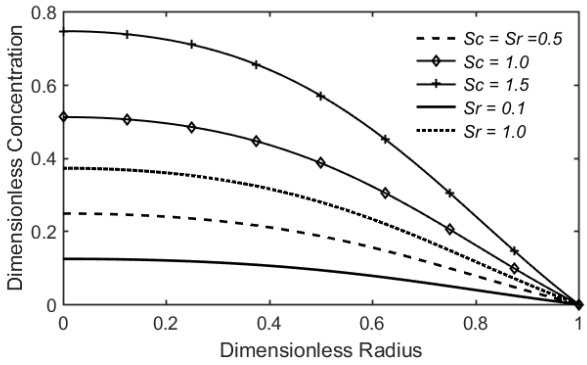

FIG. 16: Mass distribution for specific values of Sr and Sc.

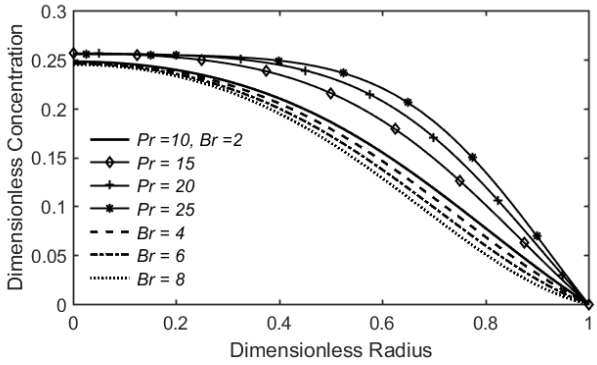

FIG. 17: Mass distribution for specific values of Pr and Br.

VII. CONCLUSION

The investigation in this paper focused on the complexities of heat and mass transfer in blood flow via a stenotic permeable channel in the presence of an external magnetic field. The Cross-fluid model, which gives a more realistic depiction of blood's non-Newtonian features, was used to characterise its rheological behavior. The problem was addressed via the fundamental equation of fluid dynamics and then normalised using dimensionless variables. The assumption of moderate stenosis was made to simplify the analysis, allowing a reduced system of equations that have been numerically solved using a finite difference approach. The effects of various emergent parameters were investigated using extensive numerical simulations, which have been discovered to have a considerable impact on important flow characteristics. The following summarises the key conclusions of this study:

- Our investigation revealed that the magnetic field, the severity of stenosis, the Weissenberg number, and the power law index all had an adverse impact on blood velocity in a stenotic artery. Such insights deepen our understanding of the elements affecting blood flow in stenotic arteries and have the potential to impact the development of cardiovascular disease-related medical technologies and treatments.

- The volume flow rate in the stenotic region was also affected by the emerging parameters, and it came down drastically by increasing the altitude of stenosis. In addition, the higher magnetic field intensities and the evaluation of the power law index and Weissenberg number led to a decrease in the flow rate magnitude. In contrast, a rise in the porosity of the vessel walls induces an increase in the magnitude of the flow rate.

- The Weissenberg number, power law index, and porosity of the vessel wall all exhibited a positive correlation with WSS, illustrating greater WSS in the stenosed segment. However, the intensity of stenosis and magnetic field magnitude had an inverse association with WSS, which caused diminished WSS. These findings highlight the importance of incorporating these parameters when assessing the effect of blood flow on wall shear stress in stenotic porous arteries.

- Flow resistance has been reported to rise significantly with stenosis height. Furthermore, it diminished with elevated wall porosity, power-law index, and Weissenberg number while increasing with magnetic field intensity. This is due to the impact of these parameters on the pressure gradient and fluid elasticity.

- The altitude of stenosis and the rise of the Brinkman number have been observed to sharply elevate the temperature profile. The Prandtl number, however, has been found to effectively reduce it.

- It has been noticed that the Schmidt and Soret numbers have profound effects on mass transport, and the higher values of both numbers lead to an increase in mass concentration. Additionally, Prandtl and Brinkman's numbers play significant roles in mass transportation. Prandtl numbers are useful for increasing mass diffusion into the stenosed region because they decrease viscous forces, whereas Brinkman numbers are useful for

increasing viscous forces and restricting mass diffusion.

- Minor amendments to temperature and concentration behaviour have been observed with adjustments in magnetic fields, porosity, and rheological parameters. Yet, these adjustments cannot be overlooked when it comes to managing temperature and concentration in blood circulation.

DECLARATION OF COMPETING INTEREST

The authors declare that they have no conflict of interest.

ACKNOWLEDGMENTS

None. The study received no external funding.

REFERENCES

[1]D. F. Young, "Fluid mechanics of arterial stenoses," Journal of Biomechanical Engineering **101**, 157–175 (1979).
[2]J. C. Misra and S. Chakravarty, "Flow in arteries in the presence of stenosis," Journal of Biomechanics **19**, 907–918 (1986).
[3]C. M. Schirmer and A. M. Malek, "Computational fluid dynamic characterization of carotid bifurcation stenosis in patient-based geometries," Brain and Behavior **2**, 42–52 (2012).
[4]K. Perktold and R. Peter, "Numerical 3D-simulation of pulsatile wall shear stress in an arterial T-bifurcation model," Journal of Biomedical Engineering **12**, 2–12 (1990).
[5]S. McGinty, "A decade of modelling drug release from arterial stents," Mathematical Biosciences **257**, 80–90 (2014).
[6]F. Yilmaz and M. Y. Gundogdu, "A critical review on blood flow in large arteries; relevance to blood rheology, viscosity models, and physiologic conditions," Korea-Australia Rheology Journal **20**, 197–211 (2008).
[7]S. Kumar and C. Diwakar, "A mathematical model of power law fluid with an application of blood flow through an artery with stenosis," Advances in Applied Mathematically Bio-Sciences **4**, 51–61 (2013).
[8]N. Ali, A. Zaman, and M. Sajid, "Unsteady blood flow through a tapered stenotic artery using Sisko model," Computers & Fluids **101**, 42–49 (2014).
[9]S. Priyadharshini and R. Ponalagusamy, "Biorheological model on flow of Herschel-Bulkley fluid through a tapered arterial stenosis with dilatation," Applied Bionics and Biomechanics **2015**, 406195 (2015).
[10]N. S. Akbar, "Non-Newtonian model study for blood flow through a tapered artery with a stenosis," Alexandria Engineering Journal **55**, 321–329 (2016).
[11]K. Subbarayudu, S. Suneetha, and P. B. A. Reddy, "The assessment of time dependent flow of Williamson fluid with radiative blood flow against a wedge," Propulsion and Power Research **9**, 87–99 (2020).
[12]M. G. Rabby, A. Razzak, and M. M. Molla, "Pulsatile non-Newtonian blood flow through a model of arterial stenosis," Procedia Engineering **56**, 225–231 (2013).
[13]S. Nadeem and N. S. Akbar, "Simulation of the second grade fluid model for blood flow through a tapered artery with a stenosis," Chinese Physics Letters **27**, 068701 (2010).
[14]R. Ahmad, A. Farooqi, R. Farooqi, N. N. Hamadneh, M. Fayz-Al-Asad, I. Khan, and M. F. Saleem Khan, "An analytical approach to study the blood flow over a nonlinear tapering stenosed artery in flow of Carreau fluid model," Complexity **2021**, 1–11 (2021).
[15]S. O. Adesanya, S. O. Ajala, and R. O. Ayeni, "A numerical study of the hemodynamics of stenosed artery," Journal of the Nigerian Association of Mathematical Physics **15** (2009).
[16]S. Kumar, B. R. Kumar, S. K. Rai, and O. Shankar, "Effect of rheological models on pulsatile hemodynamics in a multiply afflicted descending human aortic network," Computer Methods in Biomechanics and Biomedical Engineering , 1–28 (2023).
[17]H. A. Barnes, J. F. Hutton, and K. Walters, *An Introduction to Rheology* (Elsevier, 1989).
[18]V. P. Rathod and S. Tanveer, "Pulsatile flow of couple stress fluid through a porous medium with periodic body acceleration and magnetic field," Bulletin of the Malaysian Mathematical Sciences Society **32** (2009).
[19]C. Midya, G. C. Layek, A. S. Gupta, and T. R. Mahapatra, "Magnetohydrodynamic viscous flow separation in a channel with constrictions," Journal of Fluids Engineering **125**, 952–962 (2003).
[20]A. Zaman, N. Ali, and O. A. Bég, "Unsteady magnetohydrodynamic blood flow in a porous-saturated overlapping stenotic artery—numerical modeling," Journal of Mechanics in Medicine and Biology **16**, 1650049 (2016).
[21]J. Awrejcewicz, A. A. Zafar, G. Kudra, and M. B. Riaz, "Theoretical study of the blood flow in arteries in the presence of magnetic particles and under periodic body acceleration," Chaos, Solitons & Fractals **140**, 110204 (2020).
[22]B. K. Mishra and S. S. Shekhawat, "Magnetic effect on blood flow through a tapered artery with stenosis," Acta Ciencia Indica Mathematics **33**, 295 (2007).
[23]Z. Abbas, M. S. Shabbir, and N. Ali, "Numerical study of magnetohydrodynamic pulsatile flow of Sutterby fluid through an inclined overlapping arterial stenosis in the presence of periodic body acceleration," Results in Physics **9**, 753–762 (2018).
[24]I. M. Eldesoky, M. H. Kamel, R. M. Hussien, and R. M. Abumandour, "Numerical study of unsteady MHD pulsatile flow through porous medium in an artery using generalized differential quadrature method (GDQM)," International Journal of Materials, Mechanics and Manufacturing **1**, 200–206 (2013).
[25]C. G. Caro, J. M. Fitz-Gerald, and R. C. Schroter, "Atheroma and arterial wall shear-observation, correlation and proposal of a shear dependent mass transfer mechanism for atherogenesis," Proceedings of the Royal Society of London. Series B. Biological Sciences **177**, 109–133 (1971).
[26]C. R. Ethier, "Computational modeling of mass transfer and links to atherosclerosis," Annals of Biomedical Engineering **30**, 461–471 (2002).
[27]L. H. Back, J. R. Radbill, and D. W. Crawford, "Analysis of oxygen transport from pulsatile, viscous blood flow to diseased coronary arteries of man," Journal of Biomechanics **10**, 763–774 (1977).
[28]S. Charm, B. Paltiel, and G. S. Kurland, "Heat transfer coefficients in blood flow," Biorheology **5**, 133–145 (1968).
[29]P. R. Sharma, S. Ali, and V. K. Katiyar, "Mathematical modeling of heat transfer in blood flow through stenosed artery," Journal of Applied Sciences Research **7**, 68–78 (2011).
[30]A. Sinha, J. C. Misra, and G. C. Shit, "Effect of heat transfer on unsteady MHD flow of blood in a permeable vessel in the

presence of non-uniform heat source," Alexandria Engineering Journal **55**, 2023–2033 (2016).

[31]A. Zaman, N. Ali, O. A. Bég, and M. Sajid, "Heat and mass transfer to blood flowing through a tapered overlapping stenosed artery," International Journal of Heat and Mass Transfer **95**, 1084–1095 (2016).

[32]A. M. Abd-Alla, S. M. Abo-Dahab, E. N. Thabet, F. S. Bayones, and M. A. Abdelhafez, "Heat and mass transfer in a peristaltic rotating frame Jeffrey fluid via porous medium with chemical reaction and wall properties," Alexandria Engineering Journal **66**, 405–420 (2023).

[33]M. S. Dada and F. Alamu-Awoniran, "Heat and mass transfer in micropolar model for blood flow through a stenotic tapered artery," Applications and Applied Mathematics: An International Journal (AAM) **15**, 24 (2020).

[34]A. Nakayama and F. Kuwahara, "A general bioheat transfer model based on the theory of porous media," International Journal of Heat and Mass Transfer **51**, 3190–3199 (2008).

[35]V. Nasha and S. Kumar, "MHD two-layered blood flow under effect of heat and mass transfer in stenosed artery with porous medium," Applications and Applied Mathematics: An International Journal (AAM) (2021).

[36]C. Kumawat, B. K. Sharma, Q. M. Al-Mdallal, and M. Rahimi-Gorji, "Entropy generation for MHD two phase blood flow through a curved permeable artery having variable viscosity with heat and mass transfer," International Communications in Heat and Mass Transfer **133**, 105954 (2022).

[37]X. Wang, Y. Qiao, H. Qi, and H. Xu, "Numerical study of pulsatile non-Newtonian blood flow and heat transfer in small vessels under a magnetic field," International Communications in Heat and Mass Transfer **133**, 105930 (2022).